# A Karush-Kuhn-Tucker approach to field-weakening for Surface-Mounted Permanent Magnets Synchronous Motors.

Hiba Houmsi, Federico Bribiesca Argomedo, Paolo Massioni, Romain Delpoux

# A Karush-Kuhn-Tucker approach to field-weakening for Surface-Mounted Permanent Magnets Synchronous Motors

Hiba Houmsi
*Univ Lyon, INSA Lyon, Université Claude Bernard Lyon 1, Ecole Centrale de Lyon, CNRS, Ampère, UMR5005*
69621 Villeurbanne, France
hiba.houmsi@insa-lyon.fr

Federico Bribiesca-Argomedo
*Univ Lyon, INSA Lyon, Université Claude Bernard Lyon 1, Ecole Centrale de Lyon, CNRS, Ampère, UMR5005*
69621 Villeurbanne, France
federico.bribiesca-argomedo@insa-lyon.fr

Paolo Massioni
*Univ Lyon, INSA Lyon, Université Claude Bernard Lyon 1, Ecole Centrale de Lyon, CNRS, Ampère, UMR5005*
69621 Villeurbanne, France
paolo.massioni@insa-lyon.fr

Romain Delpoux
*Univ Lyon, INSA Lyon, Université Claude Bernard Lyon 1, Ecole Centrale de Lyon, CNRS, Ampère, UMR5005*
69621 Villeurbanne, France
romain.delpoux@insa-lyon.fr

***Abstract*—This article presents a feedforward analytical solution of Field-Weakening (FW) for Surface-Mounted Permanent Magnets Synchronous Motor (SPMSM) using Karush-Kuhn-Tucker (KKT) optimality conditions. The generated current references take into consideration voltage and current constraints, load torque, and speed references. The formulated optimization problem helps ensure that the generated references stays within the feasible domain given by the constraints. Furthermore, the solution given by the KKT is implemented in real-time using a low cost rapid control prototyping microcontroller (ATSAME54P20A) without the use of look-up tables.**

***Index Terms*—Flux-weakening control, Karush-Kuhn-Tucker (KKT), surface-mounted permanent magnet synchronous motor (SPMSM), real-time control, rapid control prototyping.**

## I. Introduction

Electrical Vehicles [1], Robotics [2], Power generation [3] and other industries use Surface-Mounted Permanent Magnets Synchronous Motors (SPMSMs). This is thanks to their high power density, high efficiency, ease to manufacture and compact structure. To fully take advantage of the intrinsic characteristics of SPMSMs, vector control is usually implemented. When high speed performance is required, the aforementioned control technique is augmented using ad hoc methods such as flux weakening (FW). Several approaches have been studied in the literature when it comes to field weakening techniques [4] - [10]. They can be classified into three categories: (i) feedback (ii) signal injection (iii) feedforward. Feedback control computes the current trajectories using a voltage control loop. In [4], a novel virtual speed dependent current constraint is introduced to improve the transient response of the speed loop. Paper [5] presents a gradient descent based method to alter the current reference generated by the voltage control in order to keep the problem feasible. The voltage feedback control strategy is considered robust due to the active error correction, and is usually described as model-free. Nevertheless, the model is used for proper controller tuning, antiwind-up management and bandwidth decoupling. Signal injection control strategies (Perturb & Observe) are the most model free techniques to achieve flux weakening operation. The aforementioned method comes with issues such as sensitivity to exterior perturbations, additional losses, and state ripple. Some issues related to this control are addressed, for example, in [6], [7]. Feedforward is a model-based method that computes the currents references using the mathematical model of the SPMSM. In [8] the flux weakening analytical solutions are presented for different type of electrical machines using the Lagrangian formalism. (e.g: permanent-magnet assisted machines, excited reluctance synchronous machines, interior permanent magnet synchronous machines...). Feedforward methods are usually described as computationally heavy, especially in the cases treated in [8]. To avoid cumbersome equations, iterative methods can be used [9], [10]. Paper [9] uses feedforward projected gradient descent to ensure respecting the non-linear voltage and current constraints. In [10] a Levenberg–Marquardt algorithm, is used for the same purpose. Convex optimization is used in [11] for FW and furthermore to build an optimal speed controller.

The contribution of this paper is to introduce the KKT optimality conditions methodology to solve the FW optimization problem instead of the Lagrangian. Using the KKT

enables: (i) a general way of writing and solving the FW problem, (ii) introducing two new Lagrange multipliers, also called dual variables, they express the sensitivity of the cost function with respect to changes in the constraints of an optimization problem, (iii) a model-based trajectory correction that insures the problem is always feasible via proper anti-wind up boundary choice. The model dependency weakness of this feedforward control is addressed through real-time parameter identification using [12]. Experimental results are presented to verify the feasibility of the proposed control scheme on real-time low cost embedded applications. The paper is organized as follows: Firstly, in Section II, the considered model and the associated optimization problem are presented. Next, in Section III, the FW problem is solved analytically using KKT optimality conditions. To demonstrate the efficacy of the proposed approach, experiments are conducted in Section IV. The paper concludes with Section V, which summarizes the findings and outlines future research directions.

## II. Problem statement

### A. Model of the SPMSM

Using Clarke and Park transformations [13], the SPMSM mathematical model in the d-q axis is expressed as:

$$L\frac{di_{dq}}{dt} = v_{dq} - Ri_{dq} - p\omega L\mathcal{J}i_{dq} - e_{dq}, \tag{1}$$

$$\tau = \frac{3}{2}p\phi_f i_q, \tag{2}$$

with the rotation matrix $\mathcal{J}$ given by:

$$\mathcal{J} = \begin{bmatrix} 0 & -1 \\ 1 & 0 \end{bmatrix}, \tag{3}$$

where the Back Electromotive Force (BEMF):

$$e_{dq} = p\phi_f\omega\mathcal{J}\begin{bmatrix}1\\0\end{bmatrix} = p\phi_f\omega\begin{bmatrix}0\\1\end{bmatrix}, \tag{4}$$

and where $v_{dq} = [v_d \quad v_q]^T$ and $i_{dq} = [i_d \quad i_q]^T$ are respectively the d-q phases voltages and currents, $R$ the phase resistance, $L$ the phase inductance, $\phi_f$ the peak magnetic flux of the permanent magnets seen by a stator windings, $p$ the pole pairs number, $\omega$ the rotor angular speed, $\tau$ the electromagnetic torque.

The SPMSM is mainly subject to two constraints:

$$\|i_{dq}\|^2 = i_d^2 + i_q^2 \leq I_{max}^2, \tag{5}$$

$$\|v_{dq}\|^2 = v_d^2 + v_q^2 \leq V_{max}^2, \tag{6}$$

where $I_{max}$ and $V_{max}$ are respectively the maximum acceptable current and voltage. The $I_{max}$ magnitude mainly depends on the cooling capacity of the machine, whereas the $V_{max}$ magnitude depends on the rated voltage of the inverter and the type of modulation used. Without taking into consideration the dead-times effect and the nonlinearities of the inverter, and using sinusoidal Pulse Width Modulation (PWM): $V_{max}$ is set at $V_{dc}/2$ where $V_{dc}$ is the DC bus voltage.

### B. Formulation of the optimization problem

The desired behavior is the minimum steady state currents $i_{dq}$ to reach a given speed $\omega$ at a specific load torque $\tau$ under (5) and (6). The mathematical formulation is given by:

$$\min_{i_d,\, i_q} \quad i_d^2 + i_q^2, \tag{7a}$$

$$\text{s.t.}$$

$$L\frac{di_{dq}}{dt} = v_{dq} - Ri_{dq} - p\omega L\mathcal{J}i_{dq} - e_{dq} = 0, \tag{7b}$$

$$\|i_{dq}\|^2 = i_d^2 + i_q^2 \leq I_{max}^2, \tag{7c}$$

$$\|v_{dq}\|^2 = v_d^2 + v_q^2 \leq V_{max}^2, \tag{7d}$$

$$i_q = \frac{2}{3}\frac{\tau}{p\phi_f}. \tag{7e}$$

Substituting (7b) in (7d), we reformulate the voltage constraint into the d-q current frame, the optimization problem becomes:

$$\min_{i_d,\, i_q} \quad i_d^2 + i_q^2, \tag{8a}$$

$$\text{s.t.}$$

$$i_d^2 + i_q^2 \leq I_{max}^2, \tag{8b}$$

$$(i_d + a(\omega))^2 + (i_q + b(\omega))^2 \leq c(\omega), \tag{8c}$$

$$i_q = \frac{2}{3}\frac{\tau}{p\phi_f}. \tag{8d}$$

where $\Gamma = \{\omega, \tau, V_{max}, I_{max}\}$ is the parameters set, and

$$\begin{cases} K(\omega) = \frac{p\omega\phi_f}{R^2+(p\omega L)^2}, \\ a(\omega) = K(\omega)p\omega L, \\ b(\omega) = K(\omega)R, \\ c(\omega) = \frac{V_{max}^2}{R^2+(pL\omega)^2}. \end{cases} \tag{9}$$

The constraints presented in (8) are depicted in Fig. 1; in blue, the current constraint (8b); in yellow, purple, orange full lines the voltage constraint (8c) for three different speeds $(\omega_3, \omega_2, \omega_1)$ and in dashed lines three different torque constraints (8d).

### C. KKT optimality conditions

The problem (8) may be solved using a general Lagrange function including the inequality constraints and the KKT optimality conditions, rather than only including the equality constraints as in [10], [14], [15] and [16]. The given Lagrange function, where $\lambda$, $\mu_1$ and $\mu_2$ are the Lagrange multipliers, is:

$$\begin{aligned} &\mathcal{L}(i_d, i_q, \lambda, \mu_1, \mu_2) = \\ &i_d^2 + i_q^2 + \lambda(i_q - \tfrac{2}{3}\tfrac{\tau}{p\phi_f}) + \mu_1(i_d^2 + i_q^2 - I_{max}^2) \\ &+\mu_2\Big((i_d + a(\omega))^2 + (i_q + b(\omega))^2 - c(\omega)\Big). \end{aligned} \tag{10}$$

The Karush-Kuhn-Tucker (KKT) necessary optimality conditions can be extracted by differentiating the Lagrange function with respect to each of its variables:

$$\begin{cases} \begin{bmatrix} \frac{\partial \mathcal{L}}{\partial i_d} \\ \frac{\partial \mathcal{L}}{\partial i_q} \end{bmatrix} = \begin{bmatrix} i_d + \mu_1 i_d + (i_d + a(\omega))\mu_2 \\ 2i_q + \lambda + 2\mu_1 i_q + 2\mu_2(i_q + b(\omega)) \end{bmatrix} = 0, & \text{(11a)} \\ \begin{bmatrix} \mu_1 & \mu_2 \end{bmatrix} \begin{bmatrix} i_d^2 + i_q^2 - I_{max}^2 \\ (i_d + a(\omega))^2 + (i_q + b(\omega))^2 - c(\omega) \end{bmatrix} = 0, & \text{(11b)} \\ i_q - \dfrac{2\tau}{3p\phi_f} = 0, & \text{(11c)} \\ i_d^2 + i_q^2 - I_{max}^2 \leq 0, & \text{(11d)} \\ (i_d + a(\omega))^2 + (i_q + b(\omega))^2 - c(\omega) \leq 0, & \text{(11e)} \\ \mu_1 \geq 0, & \text{(11f)} \\ \mu_2 \geq 0. & \text{(11g)} \end{cases}$$

For a set of parameters $\Gamma = \{(\omega, \tau, V_{max}, I_{max}) \in \mathbb{R}_+^4\}$. Using system (11), four cases are considered in Tab. I.

TABLE I: Possible cases of constraints

| $\mu_1$ | $\mu_2$ | ***Active constraints*** | ***Case*** |
|---|---|---|---|
| Inactive | Inactive | None | 1 |
| Inactive | Active | Voltage | 2 |
| Active | Inactive | Current | 3 |
| Active | Active | Voltage and Current | 4 |

The voltage constraint (8c) is dependent on the speed $\omega$ of the SPMSM. It is a circle of center $(-a(\omega), -b(\omega))$ and of radius $\sqrt{c(\omega)}$. At high speed, the available torque (or $i_q$ current) decreases because of the BEMF (4) leading to voltage saturation. Hence, a negative $i_d$ current is applied to reduce the effect of the BEMF, this is called Field-Weakening. The current constraint is a steady circle of center $(0, 0)$ and radius $I_{max}$. Cases $1, 2$ from Tab. I are to be studied because they determine whether FW is necessary. Cases $3, 4$ are suitable to determine the feasibility of (11) for the given set of parameters and furthermore provide a feasible solution.

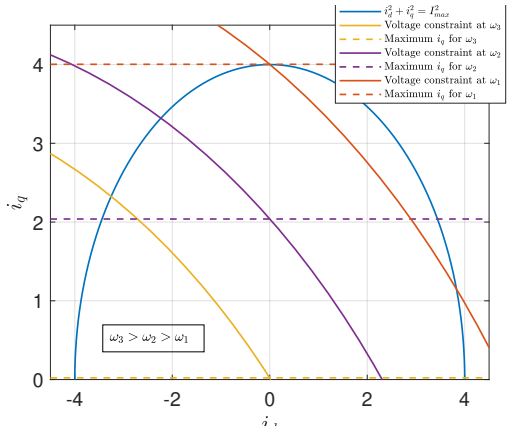


Fig. 1: Constraints in the dq-axis current plane.

## III. Analytical solutions of the optimization problem

In this section, an analytical solution to the system (11) is introduced for the four cases presented in Tab. I. The main goal is to determine the necessary $i_d$ for the set of parameters $\Gamma$. A geometrical solution is given in Fig. 2. In full purple and blue lines are represented respectively the voltage and current constraints. For a given speed $\omega$, four different torque limits are considered. First, $\tau_1$ the maximum torque without FW, it is given by the intersection between the voltage constraint and the q-axis. Then $\tau_2$, the maximum torque with FW, it is given by the intersection between the voltage and current constraints. Then $\tau_3$, the maximum torque at low speeds $\omega < \omega_1$, it is a function of $I_{max}$. Finally, $\tau_4$ the maximum torque when the voltage constraint is more restraining than the current constraint. Since the voltage constraint is speed dependent (8c), the boundaries $\tau_1, \tau_2$ and $\tau_4$ are too. Solving (11) is determining the value of $i_{dq}$ by comparing $\tau$ to the boundaries $\tau_1, \tau_2, \tau_3$ and $\tau_4$.

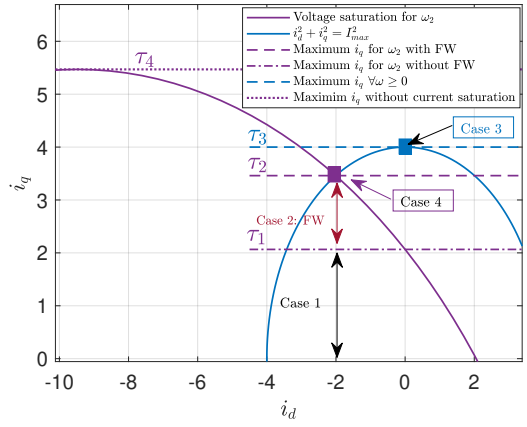


Fig. 2: Geometrical solution.

### A. Case 1: no active constraint

First, we consider the case where no inequality constraint is active. The SPMSM is in a low speed regime, meaning that the BEMF is not significant enough to reach the voltage saturation and the demanded torque does not induce current saturation. By solving the system (11), the solution is:

$$\begin{cases} i_d = 0, & \text{(12a)} \\ i_q = -\lambda = \dfrac{2\tau}{3p\phi_f}, & \text{(12b)} \\ \mu_1 = \mu_2 = 0, & \text{(12c)} \end{cases}$$

for the set of parameters given by:

$$\begin{aligned} &\Gamma_1 = \{(\omega, \tau, V_{max}, I_{max}) \in \mathbb{R}_+^4 | \\ &0 < \tau < \tau_1 = \tfrac{3}{2}p\phi_f \left( \sqrt{c(\omega) - a^2(\omega)} - b(\omega) \right) \text{ and} \\ &0 < \tau < \tau_3 = \tfrac{3}{2}p\phi_f I_{max} \text{ and } c(\omega) - a^2(\omega) \geq 0\}. \end{aligned} \quad \text{(13)}$$

The first inequality expresses the maximum available torque without FW for a range of speed $\omega \in [\omega_1, \omega_3]$ represented

in Fig. 1. Using the same inequality, we can define some notable points depicted in Fig. 1 where all full lines are voltage constraints for a particular speed, and dashed lines in the same color are the corresponding maximum achievable torque without FW. Solving: $\sqrt{c(\omega)-a^2(\omega)}-b(\omega)=I_{max}$, gives the base speed $\omega_1$ (full orange line). When $\omega>\omega_1$ the maximum rated torque given by $\tau_3=\frac{3}{2}p\phi_f I_{max}$ is no longer possible. Secondly, solving $\sqrt{c(\omega)-a^2(\omega)}-b(\omega)=0$ gives the critical speed $\omega_3$ (in yellow). When $\omega>\omega_3$, FW is compulsory to produce any torque. In purple, an intermediate point to underline the effect of the BEMF on the available torque when FW is not introduced. The Lagrange multiplier $\lambda$ conveys the sensitivity of the cost function in regard to the torque constraint. The boundaries $\tau_1$ and $\tau_3$ are schematized in Fig. 2. When $c(\omega)-a^2(\omega)\geq 0$ an intersection between the voltage constraint and the q-axis exists.

### *B. Case 2: active voltage constraint*

In case 2, the voltage constraint is active, in other terms the injection of a negative $i_d$ current is compulsory to achieve the desired torque and speed operating point. Below, the solution to (11) when the voltage constraint is active:

$$\begin{cases} i_{d\pm} = \pm\sqrt{c(\omega)-\left(\dfrac{2\tau}{3p\phi_f}+b(\omega)\right)^2}-a(\omega), & \text{(14a)}\\ i_q = \dfrac{2\tau}{3p\phi_f}, & \text{(14b)}\\ \lambda = -2i_q-2\mu_2(i_q+b(\omega)), & \text{(14c)}\\ \mu_2 = -\dfrac{i_d}{i_d+a(\omega)}>0,\ \mu_1=0. & \text{(14d)} \end{cases}$$

for the set of parameters given by:

$$\begin{aligned}\Gamma_2=\Big\{&(\omega,\tau,V_{max},I_{max})\in\mathbb{R}^4_+|\\ &\tau_1\leq\tau\leq\tau_2 \text{ and } \tau_1\leq\tau<min(\tau_3,\tau_4)\\ &\tau_4=\tfrac{3p\phi_f}{2}(\sqrt{c}-b)\}.\end{aligned} \tag{15}$$

When the voltage constraint is active, the $i_{d-}$ current given by (14a) is to be applied. The $i_q$ current is determined by $\tau$. The set $\Gamma_2$ is used for trajectory correction, as detailed later in III-E. The Lagrange multiplier $\mu_2$ denotes the sensitivity of the copper losses to the variation in the voltage constraint. The first inequality of the set $\Gamma_2$ expresses the maximum torque available seeing only the voltage constraint, Fig. 2. This is useful when the voltage constraint circle is completely included in the current constraint. The second inequality means that the demanded torque needs to be lower than the intersection between the torque given by the voltage and current constraints. This is investigated in the fourth case. The different boundaries defining the set $\Gamma_2$ are depicted in Fig. 2. An explicit formulation of $\tau_2$ is given in III-D.

### *C. Case 3: active current constraint*

In case 3, only the current constraint is active, which suggests that the demanded torque is such that $i_q=I_{max}$. When the current constraint is active, the maximum attainable speed is the base speed, $\omega_1$ discussed in III-A.

$$\begin{cases} i_d=0, & \text{(16a)}\\ i_q=\dfrac{2\tau}{3p\phi_f}=I_{max}, & \text{(16b)}\\ \lambda=-2i_d-2\mu_1 i_q & \text{(16c)}\\ \mu_1\geq 0,\ \mu_2=0 & \text{(16d)} \end{cases}$$

for the set of parameters given by:

$$\Gamma_3=\{(\omega,\tau,V_{max},I_{max})\in\mathbb{R}^4_+|\tau=\tau_3\}. \tag{17}$$

This solution is represented in Fig. 2 by the blue curves. The dual variable $\mu_1$ and $\lambda$ are linearly dependent, it implies that the corresponding constraints in the primal problem are equivalent. Here, the torque constraint is redundant with the current constraint. To draw an analogy with mechanics, it could be described as a hyperstatic situation. Thus, any value of lambda that results in a positive $\mu_1$ can be utilized to measure the sensitivity of the copper losses concerning the current constraint.

### *D. Case 4: active voltage and current constraint*

As stated in the introduction of this section, case 4 is studied to have better understanding of the steady state regime of the SPMSM, and therefore guarantee that the generated vector $i_{dq}$ is always feasible. Here, both the voltage and current constraints are active, the solution is consequently a single point given by the intersection between the two constraints, as shown by the purple square in Fig. 2. When the set $\{\omega,\tau,V_{max},I_{max}\}$ is not feasible, this point is used to determine the highest speed possible for the demanded torque, as shown in Fig. 3. The intersection between the voltage and the current constraints is given by the solution to the set of equations (11):

$$\begin{cases} i_d=\kappa_1+\kappa_2\dfrac{-2\kappa_1\kappa_2+\sqrt{\Delta}}{2(\kappa_2^2+1)}, & \text{(18a)}\\ i_q=\dfrac{2\tau_2}{3p\phi_f}=\dfrac{-2\kappa_1\kappa_2+\sqrt{\Delta}}{2(\kappa_2^2+1)}, & \text{(18b)}\\ \mu_1=-1+\dfrac{1}{2}\dfrac{(i_d+a(\omega))}{b(\omega)i_d-a(\omega)i_q}\lambda>0 & \text{(18c)}\\ \mu_2=\dfrac{i_d}{bi_d(\omega)-ai_q(\omega)}\lambda>0 & \text{(18d)} \end{cases}$$

where

$$\begin{cases} \kappa_1=\kappa_1(\omega)=\frac{(-a^2(\omega)-b^2(\omega)+c(\omega)-I^2_{max})}{2a(\omega)},\\ \kappa_2=\kappa_2(\omega)=\frac{-b(\omega)}{a(\omega)},\\ \Delta=4(I^2_{max}(\kappa_2^2+1)-\kappa_1^2), \end{cases} \tag{19}$$

for the set of parameters given by:

$$\begin{aligned}\Gamma_4=\{&(\omega,\tau,V_{max},I_{max})\in\mathbb{R}^4_+|\\ &\tau=\tau_2=\tfrac{3p\phi_f}{2}\tfrac{-2\kappa_1\kappa_2+\sqrt{\Delta}}{2(\kappa_2^2+1)}\}.\end{aligned} \tag{20}$$

Similarly to III-C, $\mu_1$ and $\mu_2$ are linearly dependent to $\lambda$, thus any value of $\lambda$ that results in a positive $\mu_1$ and $\mu_2$ can be used

to measure the sensitivity of the cost function to variation of both voltage and current constraints. The torque $\tau_2$ is depicted in Fig.2. When $\Delta \geq 0$ the intersection between the current and voltage circle exists.

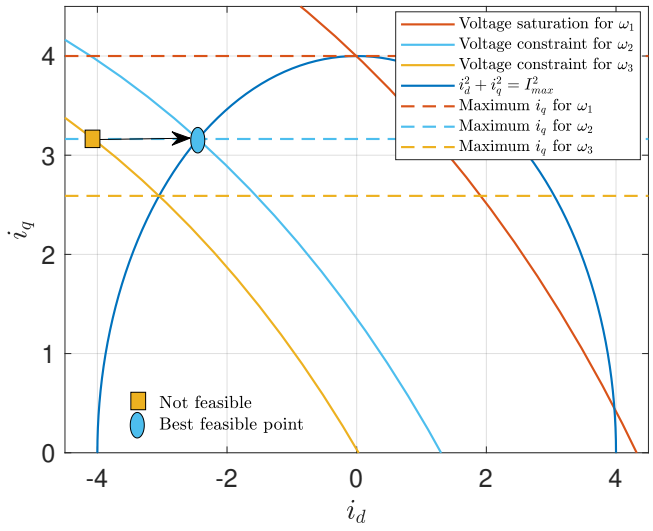


Fig. 3: Trajectory correction.

### E. Trajectory correction

When the demanded set $\Gamma$ is located outside the current constraint circle, the problem is not feasible, for instance the yellow square in Fig. 3. The aim of this section is to present a method to produce the desired torque but with the highest speed possible that respects the constraints. This idea is illustrated in Fig. 3 by the blue circle when only mechanical dry friction is considered. When viscous friction is considered, the blue circle can be lower on the current constraint. Trajectory correction uses equation (20) to choose the boundaries for the dynamic antiwind-up of the speed controller, as depicted by Fig. 4. Cases 3 and 4 are used for choosing the boundaries of the dynamic saturation bloc as detailed in algorithm 1. When the set of parameters $\Gamma$ is a subset of $\Gamma_1$ or $\Gamma_3$ no flux weakening is necessary, and the direct current is set to zero. The upper boundary of the dynamic saturation block is set to $\tau_3$. Otherwise, a negative current $i_d$ is injected to reduce the effect of the BEMF. When the boundaries of the dynamic anti-windup are reached, the speed loop is disabled (dotted lines in Fig. 4).

## IV. Experimental results

Experimental results have been carried to verify the effectiveness of the proposed control scheme on a 3-phases SPMSM. The SPMSM identified parameters are given in Tab. II. An embedded inverter demo-board from Microchip (MCLV-2), an ATSAME54P20A 32-bits microcontroller with a rapid control prototyping solution are used [17]. The inverter's switching frequency is $f_{sw} = 20$ kHz, the DC bus voltage is 24 V. Two shunt resistors and a 12 bits analog to digital converter are used for current sensing. Algorithm 1

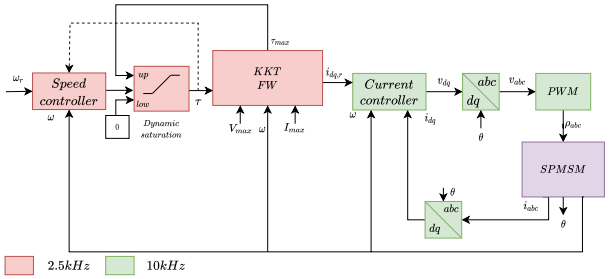


Fig. 4: The KKT flux-weakening control scheme.

**Algorithm 1** KKT FW Algorithm

**Data:** $(\tau, \omega, V_{max}, I_{max}) \in \Gamma$
**if** $\Gamma \subset \Gamma_1$ *or* $\Gamma \subset \Gamma_3$ **then**
  $i_{dr} = 0$; $\tau_{max} = \tau_3$; $i_{qr} = \frac{2\tau}{3p\phi_f}$
**else**
  $i_{dr} = \sqrt{c(\omega) - \left(\frac{2\tau}{3p\phi_f} + b(\omega)\right)^2} - a(\omega)$; $i_{qr} = \frac{2\tau}{3p\phi_f}$;
  **if** $\tau_1 < \tau_2$ & $i_{qr}^2(\tau = \tau_2) + i_{dr\_}^2(\tau = \tau_2) > I_{max}^2$ & $\Delta(\omega) > 0$ **then**
    $\tau_{max} = \tau_2$;
  **else**
    $\tau_{max} = \tau_4$;
  **end**
  **if** $\Delta(\omega) < 0$ & $i_{qr}^2(\tau = \tau_2) + i_{dr\_}^2(\tau = \tau_2) > I_{max}^2$ **then**
    $i_{dr} = NaN$; $i_{qr} = NaN$; $\tau_{max} = NaN$
  **end**
**end**

along with the speed control are implemented at a sampling frequency of $f_\omega = 2.5$ kHz. The execution time is 17.42 µs when FW is not necessary, which represents 4.35 % of the sampling period. When negative $i_d$ is injected, the execution time is 41.37 µs, which represents 10.34 % of the sampling period. The speed loop time response is 1 s. The algorithm is tested for speed steps of 10 rad/s as depicted in Fig. 5. At 430 rad/s flux weakening is necessary to stay within the voltage constraint. At 487 rad/s both voltage and current constraints are active (see Fig. 6), thus, for the torque equivalent to $i_q = 1.6$ A no higher speed than 487 rad/s is possible. When the reference speed exceeds, 487 rad/s the dynamic anti-windup deactivates the speed loop, and the maximum torque is the intersection of the voltage and current constraint. Using the measured currents and speed, it is possible to track in real time the dual variables of the KKT conditions, and therefore express the sensitivity of the cost function to the changes in

TABLE II: SPMSM parameters

| SPMSM | Values | Units |
|---|---|---|
| $R$ | 0.656 | $\Omega$ |
| $L = L_d = L_q$ | 0.35 | $mH$ |
| $\phi_f$ | 6.6 | $mWb$ |
| $p$ | 4 | - |

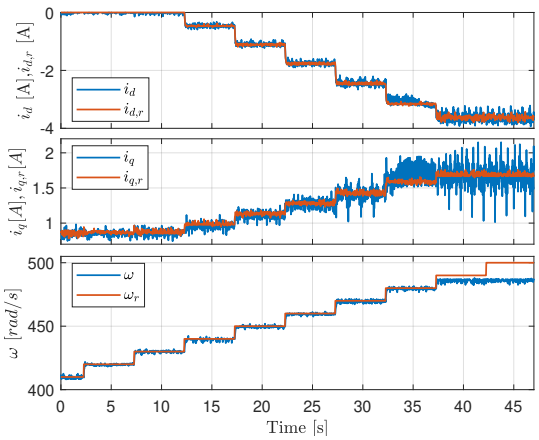


Fig. 5: Speed control. Top: the reference and measured direct current generated by the KKT FW bloc. Middle: reference and measured $i_q$ current. Bottom: reference and measured speed.

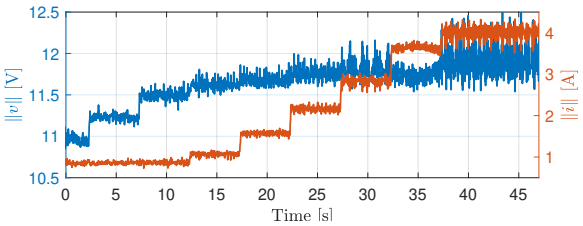


Fig. 6: Voltage and current norms.

the constraints. In the presented experiment, all constraints are active at some point. The dual variables $\lambda$, $\mu_1$ and, $\mu_2$ are depicted in Fig. 7. They indicate the direction of change in the cost function as the constraints are varied. If the dual variable for a constraint is positive, then increasing that constraint will increase the cost function, while decreasing the constraint will decrease the cost function. Conversely, if the dual variable is negative, then increasing the constraint will decrease the cost function, while decreasing the constraint will increase the cost function. This additional sensitivity information can be used as an analysis tool to gain insight into the structure of the primal problem.

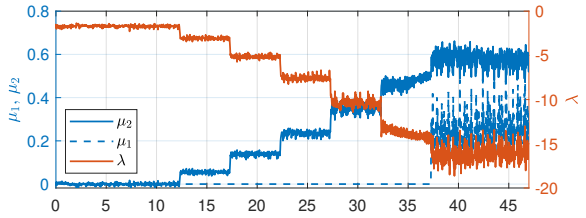


Fig. 7: Dual variables.

## V. Conclusions and Perspectives

In this paper, a novel approach to feedforward field weakening through the Karush-Kuhn-Tucker optimality conditions is introduced. This method computes the optimal currents under voltage, current, and torque constraints. Furthermore, it provides additional insight in the sensitivity of the cost function to the changes in the constraints. This sensitivity can be exploited for scaling the SPMSM, and the inverter used for the drive, moreover it can be used for scaling the SPMSM or the inverter, it can also be exploited to build a control law, which will be explored in future work. To test the proposed methodology, a control law is built and embedded on a microcontroller.

## References


[1] M. Bdewi, A. Mohammed, and M. M. Ali, "In-wheel, outer rotor, permanent magnet synchronous motor design with improved torque density for electric vehicle applications," *International Journal of Electrical and Computer Engineering (IJECE)*, vol. 12, pp. 4820–4831, Oct. 2022.

[2] J.-M. Ahn and D.-K. Lim, "Optimal Design of Surface-mounted Permanent Magnet Synchronous Motor for Robot Joint using Subdomain-Subdivide Assisted Method," in *2022 IEEE 20th Biennial Conference on Electromagnetic Field Computation (CEFC)*, pp. 1–2, Oct. 2022.

[3] H.-J. Shi and X.-C. Nie, "Composite control for disturbed direct-driven surface-mounted permanent magnet synchronous generator with model prediction strategy," *Measurement and Control*, May 2021.

[4] H. Wang, C. Gan, K. Ni, Z. Yu, and R. Qu, "Virtual Current Constraint Based Segmented Trajectory Control Strategy for Flux-Weakening Operation of SPMSM Drives," *IEEE Transactions on Power Electronics*, vol. 38, pp. 2262–2274, Feb. 2023.

[5] Y.-D. Yoon, "New Flux Weakening Control for Surface Mounted Permanent Magnet Synchronous Machine Using Gradient Descent Method," 2007.

[6] N.-Z. Jin, "Virtual Signal Injection Maximum Torque per Ampere Control Based on Inductor Identification," 2022.

[7] L. Koraqi and M. Koteich, "Torque Maximization Control of Permanent Magnet Synchronous Motors Using a Two-Stage Virtual Signal Injection," in *INDEL*, pp. 1–5, Nov. 2022.

[8] H. Eldeeb, C. M. Hackl, L. Horlbeck, and J. Kullick, "A unified theory for optimal feedforward torque control of anisotropic synchronous machines," *International Journal of Control*, vol. 91, pp. 2273–2302, Oct. 2018.

[9] Z. Xia, S. R. Filho, D. Xiao, G. Fang, Y. Sun, J. Wiseman, and A. Emadi, "Computation-Efficient Online Optimal Tracking Method for Permanent Magnet Synchronous Machine Drives for MTPA and Flux-Weakening Operations," *IEEE Journal of Emerging and Selected Topics in Power Electronics*, vol. 9, pp. 5341–5353, Oct. 2021.

[10] H.-S. Kim, Y. Lee, S.-K. Sul, J. Yu, and J. Oh, "Online MTPA Control of IPMSM Based on Robust Numerical Optimization Technique," *IEEE Transactions on Industry Applications*, pp. 3736–3746, July 2019.

[11] V. Smídl, Janouš, L. Adam, and Z. Peroutka, "Direct Speed Control of a PMSM Drive Using SDRE and Convex Constrained Optimization," *IEEE Transactions on Industrial Electronics*, pp. 532–542, Jan. 2018.

[12] R. Delpoux, M. Bodson, and T. Floquet, "Parameter estimation of permanent magnet stepper motors without mechanical sensors," *Control Engineering Practice*, vol. 26, pp. 178–187, 2014.

[13] R. H. Park, "Two-reaction theory of synchronous machines generalized method of analysis-part I," *Transactions of the American Institute of Electrical Engineers*, vol. 48, pp. 716–727, July 1929.

[14] Z. Xia, S. Nalakath, R. Tarvirdilu-Asl, Y. Sun, J. Wiseman, and A. Emadi, "Online Optimal Tracking Method for Interior Permanent Magnet Machines With Improved MTPA and MTPV in Whole Speed and Torque Ranges," *IEEE Transactions on Power Electronics*, vol. 35, pp. 9753–9769, Sept. 2020.

[15] M. Preindl and S. Bolognani, "Optimal State Reference Computation With Constrained MTPA Criterion for PM Motor Drives," *IEEE Transactions on Power Electronics*, vol. 30, pp. 4524–4535, Aug. 2015.

[16] S. Wang, J. Kang, M. Degano, A. Galassini, and C. Gerada, "An Accurate Wide-Speed Range Control Method of IPMSM Considering Resistive Voltage Drop and Magnetic Saturation," *IEEE Transactions on Industrial Electronics*, vol. 67, pp. 2630–2641, Apr. 2020.

[17] R. Delpoux, L. Kerhuel, and V. Léchappé, "On Chip Rapid Control Prototyping for DC motor," *J3eA*, vol. 20, pp. 1, http://rcp.ctrl–elec.fr/, 2021.